Efficiency and Sufficiency of Ground Motion Intensity Measures in Predicting Ejecta Potential and Peak Pore Pressures

Lianne Brito i), Caroline Bessette i), Shideh Dashti ii), Abbie B. Liel iii) and Brad Wham iv)

i) Ph.D. Candidate, Dept. of Civil, Environmental, and Architectural Eng., Univ. of Colorado Boulder, Boulder, CO, USA.
ii) Associate Professor, Dept. of Civil, Environmental, and Architectural Eng., Univ. of Colorado Boulder, Boulder, CO, USA.
iii) Professor, Dept. of Civil, Environmental, and Architectural Eng., Univ. of Colorado Boulder, Boulder, CO, USA.
iv) Assistant Research Professor, Dept. of Civil, Environmental, and Architectural Eng., Univ. of Colorado Boulder, Boulder, CO, USA.

ABSTRACT

This paper presents the results of 1520, three-dimensional (3D), fully-coupled, effective-stress, finite-element simulations in OpenSees to evaluate the influence of a variety of intensity measures (IMs) on excess pore pressures and potential for surface ejecta in the free-field. The analyzed profiles showcase different layering, and vertical changes in the groundwater table. We investigate the peak excess pore water pressure ratio in the middle of the liquefiable layer (peak r_u) and the ejecta potential index (EPI) as the primary engineering demand parameters (EDPs) of interest. A total of 20 IMs are considered as candidates, which represent a range of characteristics in terms of amplitude, frequency content, and duration of seismic loading. Efficiency, sufficiency, and predictability are used as the criteria to identify high-performing IMs for predicting the EDPs of interest. Based on the results from this preliminary parametric study, the average pseudo-spectral acceleration over the period range from 20% to 200% of the initial, small-strain site fundamental period, S_{a,avg}(0.2T_{so}, 2T_{so}) is identified as a high-performing IM for peak r_u in the free-field. For EPI predictions, the high-performing IM was found to be the cumulative absolute velocity (CAV). Both IMs were on outcropping rock.

Keywords: excess pore pressure, ejecta potential, high-performing intensity measures, site response analysis

1 INTRODUCTION

In performance-based earthquake engineering (PBEE), geotechnical engineers are often tasked with assessing the risk of liquefaction triggering and its subsequent consequences. A critical part of the PBEE framework is the choice of intensity measures (IMs). Prior studies have shown how variations of excess pore pressure ratio (i.e., r_{u,mean} or r_{u,peak}), are influenced by different IMs (Kramer and Mitchell 2006; Dashti and Karimi 2016; Wu et al. 2022). Nonetheless, a significant constraint observed in previous investigations is their inability to realistically represent variable deposits that account for heterogeneity and layering, as is often found in the field. Following the Christchurch earthquakes, ignoring interlayering led to an error of 50 to 91% in predicting far-field liquefaction triggering (Cubrinovski et al. 2019).

In this study, an extensive array of IMs evaluated at the outcropping rock location is assessed concerning their predictive capability for peak excess pore pressure ratio (peak r_u) in the middle of the liquefiable layer and the potential for surface ejecta. The potential for ejecta is indirectly evaluated through an index, referred to as the ejecta potential index (EPI), that depends on the

extent of hydraulic gradients developed during dynamic loading (Hutabarat 2020). Ten individual profiles representing different layering, and vertical changes in the groundwater table in the free-field were modeled in OpenSees. Nonlinear dynamic simulations were performed on the profiles, utilizing 152 ground motion records. The engineering demand parameters (EDPs) considered are peak r_u and EPI. The different IMs are evaluated and compared for each EDP in terms of their efficiency, sufficiency, and predictability. Finally, the high-performing IMs are determined for predicting peak r_u and EPI in the free-field.

2 NUMERICAL MODELING

To identify the high-perfoming IMs for peak $\rm r_u$ and EPI in layered profiles, 3D, fully coupled, nonlinear, effective stress finite-element (FE) simulations were performed in the object-oriented, open source, FE computational OpenSees platform (Mazzoni et al. 2006). The pressure-dependent, multi-yield surface, version 2, soil constitutive model (PDMY02), was used to represent the dynamic behavior of granular soils susceptible to liquefaction (Elgamal et al. 2002; Yang et al. 2008). The soil model parameters were adopted from

Hwang et al. (2022). The calibration process was based on monotonic and cyclic, drained and undrained triaxial tests (Badanagki 2019), centrifuge test results modeling free-field soil conditions with the same soil types (Ramirez et al. 2018), and field observations (NCEER 1997). The soil column was modeled with threedimensional 20-8 node BrickUP elements. Each model was divided into 48 elements with a uniform element thickness of 0.5 m. The fluid bulk modulus was assumed to be 2.2 x 10⁶ kPa at atmospheric pressure. The displacements in all three directions located at the same elevation were tied together. Additionally, the nodes located perpendicular to shaking planes were fixed against out-of-plane (y-direction) displacements. For the models representing a dry crust, the soil nodes at or above the water table location were fixed in the fourth degree of freedom to simulate dry conditions. At the base of the model, nodes were fixed against vertical translation, and to replicate a compliant base boundary condition in the horizontal plane, a Lysmer-Kuhlemeyer (1969) dashpot was introduced. The dashpot consisted of two extra nodes in the same location as the soil base left hand corner node. One of the dashpot nodes was fixed in all directions, and the second node was fixed against vertical translation and tied to the soil base left hand corner node for horizontal translation. The dashpot was modeled with a zero-length element and assigned a viscous uniaxial material with a coefficient that is the product of the underlying bedrock layer's mass density and shear wave velocity. A mass density of 2.5 Mg/m³ and a shear wave velocity of 1000 m/s were used as the bedrock properties in all the analyses (Tiznado et al. 2021). The input motions were applied as a force time history to the base of the soil column, which was based on the velocity time history multiplied by the dashpot coefficient.

3 NUMERICAL PARAMETRIC STUDY

We performed 1520 simulations with the aid of the Alpine supercomputing facility at University of Colorado Boulder (CU). Five representative profiles were studied, varying the number of critical, loose, and saturated Ottawa sand layers and the number of low permeability silt layers distributed within the profile (see Fig. 1). In addition, the same 5 profiles were modeled with the groundwater table at the surface and at 2 m depth, resulting in 10 individual soil profiles. The selected soil profiles and groundwater table were determined based on observed trends in the Hutabarat (2020) case history database of site conditions with varying degrees of ejecta severity.

The soil profiles in Fig. 1 vary in complexity. Soil ID 1 and ID 2 represent a typical uniformly layered profile or one with the addition of a silt capping layer, both of which have been previously studied and validated with recordings from centrifuge experiments (Ramirez et al. 2018; Brito et al. 2024). In soil ID 3, we maintain both

the total thickness of the critical liquefiable layer (6 m) and the total profile thickness (24 m), while introducing 4 silt layers around and within the liquefiable layer that disrupt its continuity. In soil ID 4, we introduce multiple loose Ottawa sand layers that add to the same cumulative liquefiable thickness as IDs 1-3 (6 m) but spread out to different depths and separated by dense sand interlayers. Lastly, in soil ID 5, we introduce silt caps at the boundaries of each of the liquefiable layers in ID 4.

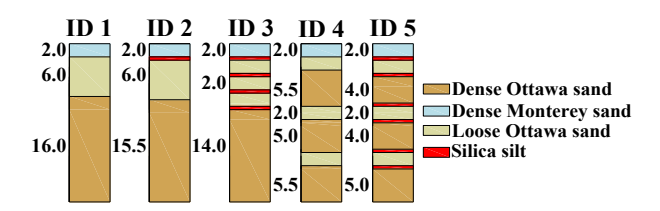


Fig. 1. Schematic of selected numerical parametric study soil profiles (dimensions are in meters).

A suite of 152 outcropping rock motions was chosen from the Bullock et al. (2017) database and used as input for each model configuration. The selected suite of ground motions was collected from NGA-West2, KiK/K-Net, NZSMD, COSMOS, RENADIC, and CSN databases, each having two horizontal components. The two horizontal recordings were rotated to find the maximum rotated (RotD100) peak ground acceleration. The ground motions were baseline-corrected and filtered (using a band-pass filter with corner frequencies of 0.1 and 12 Hz). This input ground motion set was recorded on outcropping rock ($V_{s,30} > 760 \text{ m/s}$) and encompassed 74 records from normal, reverse, and strike-slip shallow crustal earthquakes and 77 records from interface and intraslab subduction earthquakes. Fig. 2 shows the distribution of the selected ground motion records in terms of moment magnitude (M_w), distance to rupture (R_{rup}), peak ground acceleration (PGA), and cumulative absolute velocity (CAV).

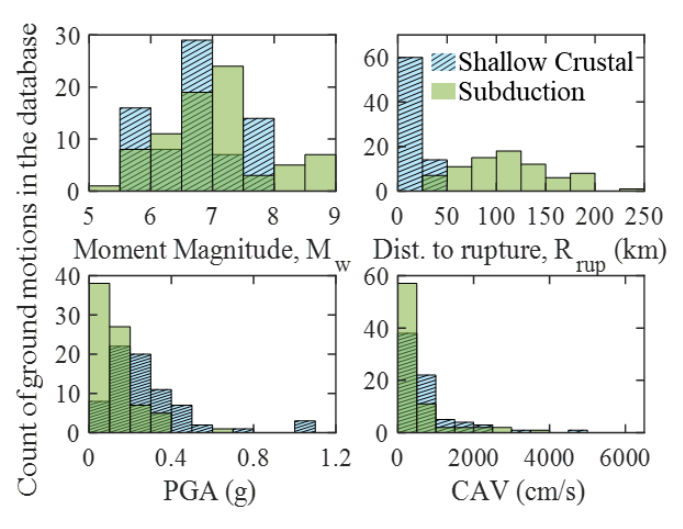


Fig. 2. Distribution of ground motion parameters as recorded at outcropping rock, employed as input in the numerical study.

Twenty IMs were evaluated as candidates, including 11 peak transient IMs, 3 evolutionary IMs, 4 durationrelated IMs, and 2 frequency-related IMs (summarized in Table 1). We evaluated these IMs in terms of their efficiency and sufficiency in predicting peak excess pore pressures in the middle of the liquefiable layer and ejecta potential, as well as their predictability following the approach of Dashti and Karimi (2016). Efficiency reflects how well an IM can predict a given EDP with no other information, and is quantified by the standard deviation of the residuals around the regression relating the IM to the EDP, denoted $\sigma_{peak ru}$ and $\sigma_{ln(EPI)}$. Sufficiency is a measure of whether the IM is independent of earthquake source characteristics. It is quantified by the slope of a linear regression line, assessing the dependence of residuals about the EDP on M_w or R_{rup}. Lastly, predictability indicates the applicability and availability of ground motion prediction equations (GMPEs) for a given IM and is quantified by the standard deviation of logarithmic IMs from the existing GMPEs. We use the outcropping rock location in this study, which is more predictable than other locations, as suggested by Bullock et al., (2019).

Table 1. Intensity measures considered in this study

Table 1. Intensity measures	considered in this study.
IM	Equation
PGA	PGA = max a(t)
PGV	$PGV = \max v(t) $
PGD	$PGV = \max u(t) $
CAV	$CAV = \int_{0}^{t_{tot}} a(t) dt $ $CAV_{5} = \int_{0}^{t_{tot}} \langle x \rangle a(t) dt$
CAV ₅	$CAV_5 = \int_0^{t_{tot}} \langle x \rangle a(t) dt$
I_a	$I_{a} = \frac{\pi}{2g} \int_{0}^{t_{tot}} a^{2}(t) dt$
D ₅₋₇₅	-
D ₅₋₉₅	-
SIR ₇₅	$SIR_{75} = \frac{0.7I_a}{D_{5-75}}$
SIR ₉₅	$SIR_{75} = \frac{0.9I_a}{D_{5-95}}$
$T_{\rm m}$	$SIR_{75} = \frac{D_{5-75}}{D_{5-75}}$ $SIR_{75} = \frac{0.9I_a}{D_{5-95}}$ $T_m = \frac{\sum c_i^2/f_i}{\sum c_i^2}$
T_p	-
ASI	ASI = $\int_{0.1}^{0.5} S_a(\xi = 5\%, T) dT$ VSI = $\int_{0.1}^{0.5} S_v(\xi = 5\%, T) dT$
VSI	$VSI = \int_{0.1}^{0.5} S_{\nu}(\xi = 5\%, T) dT$
$S_a(1.0)$	-
S _a (T _{so})	-
S _a (1.5T _{so})	-
$S_a (2.0T_{so})$	-
$S_{a,avg}(0.2T_{so}, 1.5T_{so})$	-
$S_{a,avg}(0.2T_{so}, 2.0T_{so})$	-

The EDPs under consideration are the peak excess pore water pressure ratio (peak $r_u = max\ EPWP/\sigma_{zo}$ ') in the middle of the liquefiable layer and the EPI as defined by Hutabarat (2020). For peak r_u , we consistently relied on numerically predicted excess pore pressures at the middle of the total thickness of the loose Ottawa sand layer/s (e.g., z=5 m and z=10.5 m for IDs 1 and 5, respectively). In Hutabarat's procedure, the excess pressure head required ($h_{exc}=u_e/\gamma_w$) to produce surface

ejecta manifestation corresponds to the existing excess head that exceeds the artesian excess head (h_A). This artesian excess head is depicted as a linear relationship with a 1:1 sloped line across the depth of the profile, constrained within the limits of the maximum excess head (max $h_{exc} = \sigma_{zo} / \gamma_w$). EPI is bound by the duration of artesian conditions (a minimum time when input acceleration reaches 0.05 g and a maximum of 150 s) and the upper 10 m of the profile, which is assumed to provide most of the demand. The ejecta manifestation severity is categorized as minor (10 - 40 m³·s), moderate (40 - 100 m³·s), severe (100 - 300 m³·s), and extreme (greater than $300 \text{ m}^3 \cdot \text{s}$). For the purpose of identifying a high-performing IM for predicting EPI, we evaluated only cases where the severity category of ejecta manifestation was at least minor. This filtering process resulted in the inclusion of only those cases where the groundwater table was positioned at a depth of 2 m. In other words, none of the 5 profile configurations with the groundwater table at the surface produced an EPI value greater than 10 m³·s. This resulted from the limited σ_{zo} , preventing the excess hydraulic head from reaching the limit for initiating artesian flow.

A logistic and beta regression models were employed to fit peak r_u (Dashti and Karimi 2016; Wu et al. 2022). In evaluating the efficiency and sufficiency of the IMs considered in predicting peak r_u , the results were relatively insensitive to the choice between the two regression models. Thus, for brevity, we only present the results from the logistic regression model in this paper. Similarly, for EPI in log-log scale, we employed linear and polynomial regression models, resulting in similar results. Therefore, we present only the results from the linear regression model in this paper.

4 HIGH-PERFORMING IMS FOR PEAK PORE PRESSURES EVALUATION

We utilized the set of 20 candidate IMs to perform logistic regression analyses with peak r_u evaluated in the middle of the liquefiable layer. For each IM, one $\sigma_{peak\ ru}$ can be obtained for each individual soil profile (10 data points per IM considered). Fig. 3 presents the efficiency plots for $ID1_{gwt2m}$ for a few representative outcropping rock motion IMs, highlighting $\sigma_{peak\ ru}$.

Fig. 4 summarizes the $\sigma_{peak ru}$ values for the 10 most efficient IMs (smaller values reflect higher efficiency) on outcropping rock out of 20 considered. The figure presents results for all the soil profiles considered. Arias Intensity (I_a), acceleration spectrum intensity (ASI), velocity spectrum intensity (VSI), average pseudospectral acceleration over the period range from 20% to 150% of the initial fundamental site period, $S_{a,avg}(0.2T_{so}, 1.5T_{so})$, and average pseudo-spectral acceleration over the period range from 20% to 200% of the initial site period, $S_{a,avg}(0.2T_{so}, 2T_{so})$ demonstrated higher efficiencies compared to others. These last two peak transient IMs, encompass the frequency content over a

range of periods. As highlighted by Bullock et al. (2019), this type of IM is often more effective than single-period values of S_a since the soil column's site period could change as its strength and stiffness are altered by degradation and softening during dynamic loading.

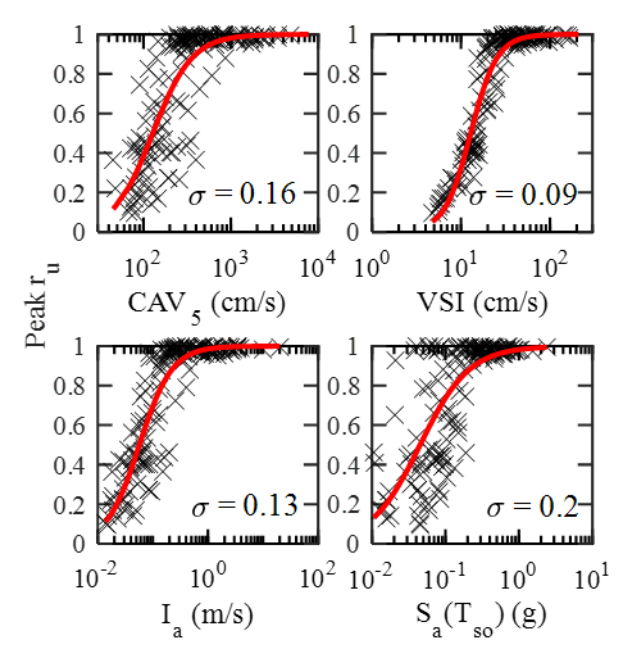


Fig. 3. Peak excess pore pressure ratio efficiency plots for $ID1_{gwt2m}$ using different outcropping rock motion IMs.

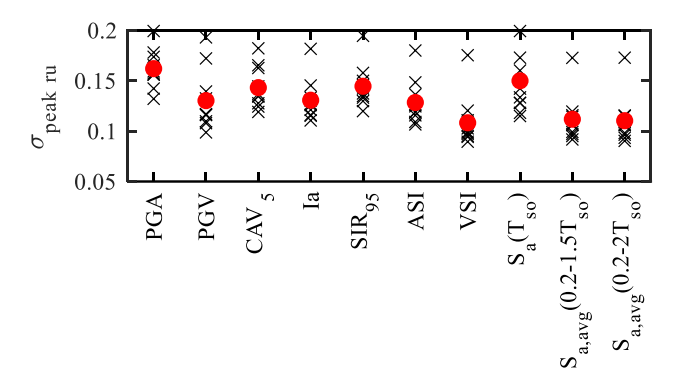


Fig. 4. Standard deviation ($\sigma_{peak\ ru}$) for the ten most efficient IMs considered. The red circles represent the mean across $\sigma_{peak\ ru}$ values for the 10 soil profiles.

To evaluate sufficiency, as previously mentioned, we examined the slope of a linear regression line (c^M and c^R) through the residuals about peak r_u with respect to M_w and R_{rup} . Fig. 5 represents this procedure for I_a in $ID1_{gwt2m}$.

For each IM, we averaged the absolute values of the slopes (c^M and c^R) from M_w and R_{rup} to obtain the c_{avg} values presented in Fig. 6. The IMs of peak ground velocity (PGV), I_a , pseudo-spectral acceleration at the sites' fundamental periods, $S_a(T_{so})$, $S_{a,avg}(0.2T_{so}, 1.5T_{so})$, and $S_{a,avg}(0.2T_{so}, 2T_{so})$ illustrate greater sufficiency with median c_{avg} values smaller than 0.02. The best combination of efficiency and sufficiency was found on

 $S_{a,avg}(0.2T_{so}, 2T_{so})$ with a median $\sigma_{peak\ ru}$ of 0.11 and a median c_{avg} of 0.017.

As stated previously, predictability needs to be considered when selecting a high-performing IM. As stated by Bullock et al. (2019), GMPEs are available for S_a across various periods and different tectonic environments. Employing the selected GMPEs they can be integrated with the correlation models of Baker and Jayaram (2008) to make predictions of $S_{a,avg}(0.2T_{so})$ 2T_{so}) as performed by Bullock et al. (2021). The small strain fundamental period of the site, T_{so}, may be estimated as $4H/\overline{V}_s$, where V_s is the average small-strain, shear wave velocity, and H is the total height of the soil column above bedrock (Dashti and Karimi 2016). More recent work by Davalos and Miranda (2021) provided GMPEs for S_{a,avg} across different periods, but only for the shallow crustal tectonic environment with a standard deviation range of 0.56-0.65. This study also highlighted how $S_{a,avg}$ is more predictable than S_a (i.e., typical standard deviation range of 0.6-0.7).

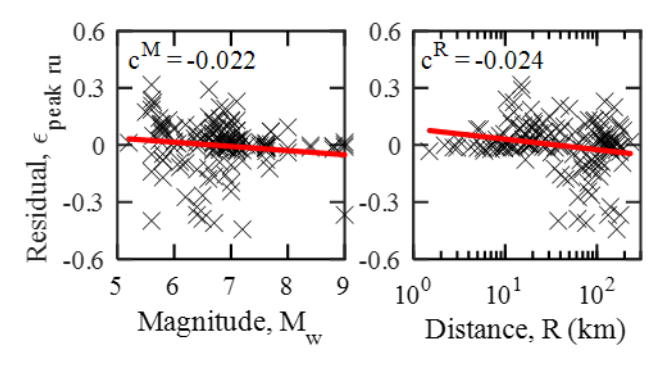


Fig. 5. Arias intensity (I_a) sufficiency with respect to source moment magnitude (M_w) and distance (R) for $ID1_{wt2m}$.

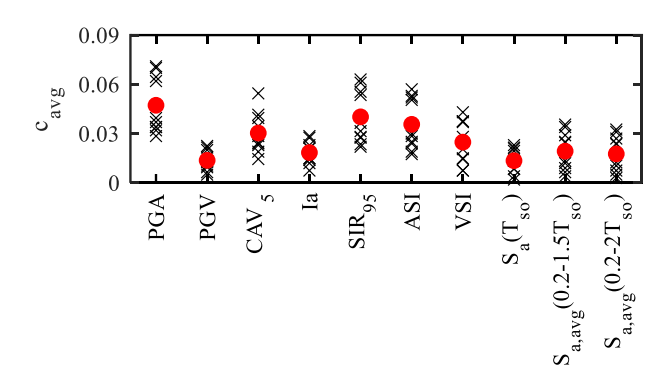


Fig. 6. Estimated c_{avg} values for the residuals of peak r_u from the ten most efficient IMs considered. The red circles represent the mean across c_{avg} values for the 10 soil profiles.

It is worth noting that the high-performing IM found for predicting peak r_u in the free-field in this study differs from the one suggested by Dashti and Karimi (2016), $S_a(T_{so})$. While only considering relatively uniform granular soil profiles, in the Dashti and Karimi (2016) study, $S_{a,avg}$ was not considered as a candidate IM.

Nonetheless, S_a(T_{so}) was identified in our results as both in the top 10 most efficient IMs and top 5 most sufficient IMs.

5 HIGH-PERFORMING IMS FOR EJECTA POTENTIAL EVALUATION

The same procedure highlighted in the previous section was employed to evaluate the high-performing IM for EPI prediction. The $\sigma_{ln(EPI)}$ values for the 10 most efficient IMs are summarized in Fig. 7. The evolutionary IMs CAV, CAV5 and I_a show the highest efficiency, with the mean $\sigma_{ln(EPI)}$ in the range of 0.48 and 0.56. The calculated values for $\sigma_{ln(EPI)}$ being larger than for $\sigma_{peak\ ru}$ are partly due to the reduction in sample size (associated with exclusion of results with no to minor ejecta potential, explained in previous sections).

Fig. 8 shows the distribution of c_{avg} dispersion, with IMs CAV and CAV₅ demonstrating the highest sufficiency with 0.08 and 0.07 mean c_{avg} , respectively. Given the prediction uncertainty ranges outlined by Bullock et al. (2019), with a standard deviation that ranges from 0.4 to 0.7 for CAV and 0.7 to 0.9 for CAV₅, CAV is deemed as the highest performing IM for predicting EPI in the free-field for the conditions evaluated.

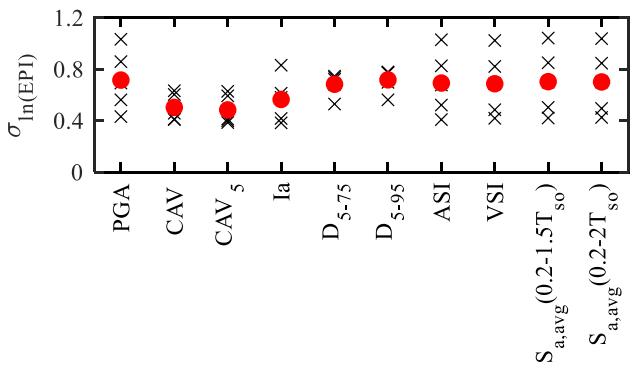


Fig. 7. Standard deviation $\sigma_{ln(EPI)}$ for the ten most efficient IMs considered.

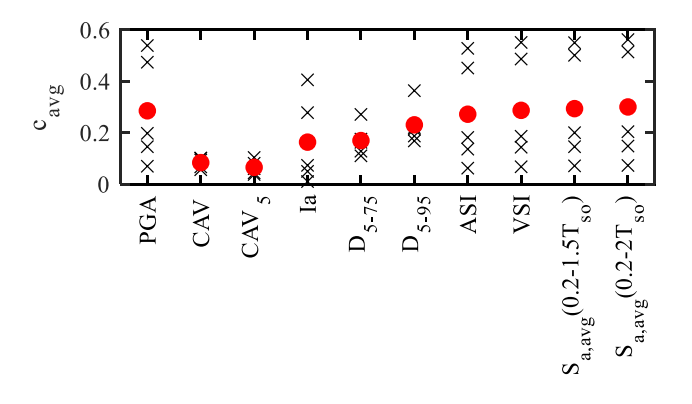


Fig. 8. Estimated $c_{\rm avg}$ values for the residuals of EPI from the ten most efficient IMs considered.

6 CONCLUSIONS

This paper describes the results of a preliminary numerical parametric study to identify potential highperforming IMs for predicting peak excess pore pressures and ejecta potential in free-field for realistic interlayered liquefiable deposits. Fully-coupled, 3D, nonlinear, effective stress finite-element analyses of realistically variable deposits were modeled in OpenSees. In each of the 10 individual soil profiles, dynamic analyses were conducted using a selection of 152 ground motions as input, resulting in 1520 simulations. Twenty IMs were adopted as the potential candidate IMs in this study. Peak r_u in the middle of the liquefiable layer and ejecta potential index (EPI) were selected as the EDPs of interest. The pool of IMs was compared in terms of efficiency, sufficiency, and predictability in predicting the EDPs of interest. We employed logistic and linear regression analyses for peak r_u and EPI, respectively, to establish relationships between the EDPs and the potential IMs. We identified the best combination of efficiency, sufficiency, and predictability in S_{a,avg}(0.2T_{so}, 2T_{so}) for peak r_u and CAV for EPI predictions in the free-field of interlayered granular and liquefiable soil deposits. These IMs were only evaluated at the outcropping rock location. Though insightful in guiding future predictive models, additional simulations are needed in the future with more variations in soil conditions, rock properties, ground motions, as well as lateral variations in soil profile. These simulations are under way by the authors.

ACKNOWLEDGEMENTS

Funding from the NSF Graduate Research Fellowship (GRFP) and the Graduate Assistance in Areas of National Need (GAANN) are gratefully acknowledged. This work utilized the Alpine high-performance computing resource at the University of Colorado Boulder. Alpine is jointly funded by the University of Colorado Boulder, the University of Colorado Anschutz, Colorado State University, and the National Science Foundation (award 2201538).

REFERENCES

- 1) Badanagki, M. (2019): Influence of dense granular columns on the seismic performance of level and gently sloped liquefiable sites, Ph.D. thesis, Univ. of Colorado Boulder.
- 2) Baker, J. W., & Jayaram, N. (2008): Correlation of spectral acceleration values from NGA ground motion models, *Earthquake Spectra*, 24(1), 299-317.
- 3) Bullock, Z., Dashti, S., Liel, A., Porter, K., Karimi, Z., & Bradley, B. (2017): Ground-motion prediction equations for Arias intensity, cumulative absolute velocity, and peak incremental ground velocity for rock sites in different tectonic environments, *Bulletin of the Seismological Society of America*, 107(5), 2293-2309.
- 4) Bullock, Z., Dashti, S., Liel, A. B., Porter, K. A., & Karimi, Z. (2019): Assessment supporting the use of outcropping rock evolutionary intensity measures for prediction of liquefaction

- consequences, Earthquake Spectra, 35(4), 1899-1926.
- 5) Bullock, Z., Dashti, S., Liel, A. B., & Porter, K. A. (2021): Can geotechnical liquefaction indices serve as predictors of foundation settlement?, *Earthquake Spectra*, 37(4), 2271-2287.
- 6) Brito, L., Bessette, C., Dashti, S., Liel, A.B., Wham, B. (2024): Influence of Stratigraphic Variability and Layering on Liquefiable Soils Near and Away from structures, *Geo-Congress*, Vancouver, Canada.
- 7) Cubrinovski, M., Rhodes, A., Ntritsos, N., & Van Ballegooy, S. (2019): System response of liquefiable deposits, *Soil Dynamics and Earthquake Engineering*, 124, 212-229.
- 8) Dashti, S., & Karimi, Z. (2017): Ground motion intensity measures to evaluate I: The liquefaction hazard in the vicinity of shallow-founded structures, *Earthquake Spectra*, 33(1), 241-276.
- 9) Dávalos, H., and Miranda, E. (2021): A Ground Motion Prediction Model for Average Spectral Acceleration, *Journal of Earthquake Engineering*, 25(2), 319–342.
- 10) Elgamal, A., Yang, Z., & Parra, E. (2002): Computational modeling of cyclic mobility and post-liquefaction site response, *Soil Dynamics and Earthquake Engineering*, 22(4), 259-271.
- 11) Hutabarat, D. (2020): Effective stress analysis of liquefaction sites and evaluation of sediment ejecta potential, Ph.D. thesis, Univ. of California, Berkeley.
- 12) Hwang, Y. W., Bullock, Z., Dashti, S., & Liel, A. (2022): A Probabilistic Predictive Model for Foundation Settlement on Liquefiable Soils Improved with Ground Densification, *Journal of Geotechnical and Geoenvironmental Engineering*, 148(5), 04022017.
- 13) Kramer, S. L., & Mitchell, R. A. (2006): Ground motion intensity measures for liquefaction hazard evaluation, *Earthquake Spectra*, 22(2), 413-438.
- 14) Lysmer, J. and Kuhlemeyer, A.M. (1969): Finite dynamic model for infinite media, *Journal of the Engineering Mechanics Division*, ASCE, 95, 859-877.
- 15) Mazzoni, S., McKenna, F., Scott, M. H., & Fenves, G. L. (2006): Open system for earthquake engineering simulation user command-language manual, *Pacific Earthquake Engineering Research Center, University of California, Berkeley, OpenSees version*, 1(3).
- 16) NCEER (1997): Proceedings of the NCEER workshop on evaluation of liquefaction resistance of soils, Technical Rep. No. NCEER-97-0022. Taipei, Taiwan.
- 17) Ramirez, J., Barrero, A. R., Chen, L., Dashti, S., Ghofrani, A., Taiebat, M., & Arduino, P. (2018): Site response in a layered liquefiable deposit: evaluation of different numerical tools and methodologies with centrifuge experimental results, *Journal of Geotechnical and Geoenvironmnetal Engineering*, 144(10), 04018073.
- 18) Tiznado, J. C., S. Dashti, and C. Ledezma. (2021): Probabilistic predictive model for liquefaction triggering in layered sites improved with dense granular columns, *Journal of Geotechnical and Geoenvironmnetal Engineering*, 147(10), 04021100.
- 19) Wu, Q., Li, D. Q., & Du, W. (2022): Identification of optimal ground-motion intensity measures for assessing liquefaction triggering and lateral displacement of liquefiable sloping grounds, *Earthquake Spectra*, 38(4), 2707-2730.
- 20) Yang, Z., Lu, J., & Elgamal, A. (2008): OpenSees soil models and solid-fluid fully coupled elements. *User's Manual. Ver*, 1, 27.